





# Geotechnical investigations and remediation design for failure of tunnel portal section: a case study in northern Turkey

**Ayberk KAYA**<sup>1\*</sup>  <http://orcid.org/0000-0001-7278-333X>;  e-mail: ayberk.kaya@erdogan.edu.tr

**Kadir KARAMAN**<sup>2</sup>  <http://orcid.org/0000-0002-3831-4465>; e-mail: kadir.karaman@ktu.edu.tr

**Fikri BULUT**<sup>3</sup>  <http://orcid.org/0000-0003-1918-0593>; e-mail: fbulut@ktu.edu.tr

\* Corresponding author

<sup>1</sup> Recep Tayyip Erdogan University, Faculty of Engineering, Department of Geological Engineering, 53100, Rize, Turkey

<sup>2</sup> Karadeniz Technical University, Faculty of Engineering, Department of Mining Engineering, 61080, Trabzon, Turkey

<sup>3</sup> Karadeniz Technical University, Faculty of Engineering, Department of Geological Engineering, 61080, Trabzon, Turkey

**Citation:** Kaya A, Karaman K, Bulut F (2017) Geotechnical investigations and remediation design for failure of tunnel portal section: a case study in northern Turkey. Journal of Mountain Science 14(6). DOI: 10.1007/s11629-016-4267-x

© Science Press and Institute of Mountain Hazards and Environment, CAS and Springer-Verlag Berlin Heidelberg 2017

**Abstract:** Mass movements are very common problems in the eastern Black Sea region of Turkey due to its climate conditions, geological, and geomorphological characteristics. High slope angle, weathering, dense rainfalls, and anthropogenic impacts are generally reported as the most important triggering factors in the region. Following the portal slope excavations in the entrance section of Cankurtaran tunnel, located in the region, where the highly weathered andesitic tuff crops out, a circular toe failure occurred. The main target of the present study is to investigate the causes and occurrence mechanism of this failure and to determine the feasible remedial measures against it using finite element method (FEM) in four stages. These stages are slope stability analyses for pre- and post-excavation cases, and remediation design assessments for slope and tunnel. The results of the FEM-SSR analyses indicated that the insufficient initial support design and weathering of the andesitic tuffs are the main factors that caused the portal failure. After installing a rock retaining wall with jet grout columns and reinforced slope benching applications, the factor of safety increased from 0.83 to 2.80. In addition to

slope stability evaluation, the Rock Mass Rating (RMR), Rock Mass Quality (Q) and New Austrian Tunneling Method (NATM) systems were also utilized as empirical methods to characterize the tunnel ground and to determine the tunnel support design. The performance of the suggested empirical support design, induced stress distributions and deformations were analyzed by means of numerical modelling. Finally, it was concluded that the recommended stabilization technique was essential for the dynamic long-term stability and prevents the effects of failure. Additionally, the FEM method gives useful and reasonably reliable results in evaluating the stability of cut slopes and tunnels excavated both in continuous and discontinuous rock masses.

**Keywords:** Portal failure; Stability analysis; Finite element method; Tunnel support design; Remedial measures Rock Mass Rating (RMR); Rock Mass Quality (Q); New Austrian Tunneling Method (NATM)

## Introduction

In spite of the rapid advances in geotechnical engineering science, still slope failures impose heavy social, economic, and environmental losses.

**Received:** 28 October 2016

**Revised:** 12 March 2017

**Accepted:** 19 April 2017

Every year worldwide, this process causes deathly casualties and remarkable direct and indirect economic losses. To reduce or prevent the failure damages, slope stability analyses and stabilization are needed and to do the best, it necessitates a clear understanding and evaluation of the processes that control the behavior of the slopes. Over the past 30 years, many governments in the world have expended notable amount of resources in appraising mass movement hazards and considerable amount of scientific studies have been performed (e.g. Guzzetti et al. 1999; Del Gaudio et al. 2000; Gardner and Sazuk 2004; Borja-Baeza et al. 2006; Sarkar and Anbalagan 2008; Ahmadi and Eslami 2011; Wang et al. 2013; Manouchehrian et al. 2014; Ju et al. 2015; Yang et al. 2016; Du et al. 2017; Wang et al. 2017).

Determining the stability of rock slopes is usually difficult because of the changeable nature of rock masses which mostly contain faults, joints, anisotropy, bedding, foliation, cleavage, and schistosity or naturally occurring discontinuities. In geotechnical engineering applications, projects related to open (e.g. slopes, tunnel portals) and underground excavations primarily require evaluation stability analysis of slopes so as to maintain the slope in stable condition within construction and operation periods. In general, slope stability is examined at different phases of field exploration with varying details. If the mass failure (not discontinuity controlled) may occur because of weathering or presence of highly jointed rock mass, the slopes fail along a cylindrical surface which is called circular failure. It is very significant to determine the position of most critical circle in analysis of such failure. In this case, the circular failures are investigated carefully using limit equilibrium or numerical techniques in order to prevent environmental losses (Wyllie and Mah 2004; Li et al. 2011).

In Turkey, a large rate of the mass movements causing monetary loss annually occurs in the eastern Black Sea region. As reported in the literature (e.g. Genc 1993; Bulut et al. 2000; Akgun and Bulut 2007; Akgun 2011; Alemdag et al. 2014, 2015; Kaya et al. 2016), the main triggering factors of mass movements that occur frequently in this region are high frequency of heavy rainfall, weathering, high steep slopes, and human activities. It should be noted that the city Artvin, which is highly

susceptible to mass movements, is located in the eastern Black Sea region. In this area, the geomorphology is characterized by a steep topography increase from mainly north to south. The incline of slope varies between 25° and 55° where the dispersed settlement is located. The fields are usually covered with soil and vegetation and rock exposures are observed mainly along the road cuts and deep valleys. Weather conditions in the city are warm and dry in summers, and cool and rainy in winters. The maximum precipitation, mainly in the form of rain occurs in autumn (between September and November). According to meteorological data (MGM 2016), the highest temperature recorded in Artvin city and the surrounding area is 22.3°C in July and the lowest temperature is 7.3°C in January. The average annual precipitation is 338.7 mm.

Due to increasing traffic load, and as a precaution to decrease traffic congestion in the coming years, the improvement of the Artvin–Hopa government highway (KM: 6+500–13+787) was adjudicated by the authorities of Turkish General Directorate of Highways (KGM). The project included the construction of the Cankurtaran Tunnel (Figure 1) comprised mainly of volcanic and sedimentary rocks and situated between KM: 7+980–KM:13+208. Towards the right tube slope (Figures 2a and 2b) of the entrance portal (KM: 7+990), a failure has occurred (before the top heading excavation of the tunnel in the right tube) 13 m behind the slope face with a width of 34 m and length of 29 m (Figures 2c and 2d). This study aims to carry out engineering geological studies including field measurements, laboratory studies, and slope/tunnel stability analyses in order to understand the causes and mechanism of the portal failure; and to determine the most economic and reliable remediation measures in order to make the portal slope and tunnel stable.

## 1 Geological Setting

Based on the lithological and structural evidence, the Eastern Pontide is subdivided into southern and northern zones (Ketin 1966). The study area is located in northern part of the Eastern Pontide Tectonic Assembly, Black Sea region, Turkey. The tectonic assembly consists of different units in varying ages, ranging from

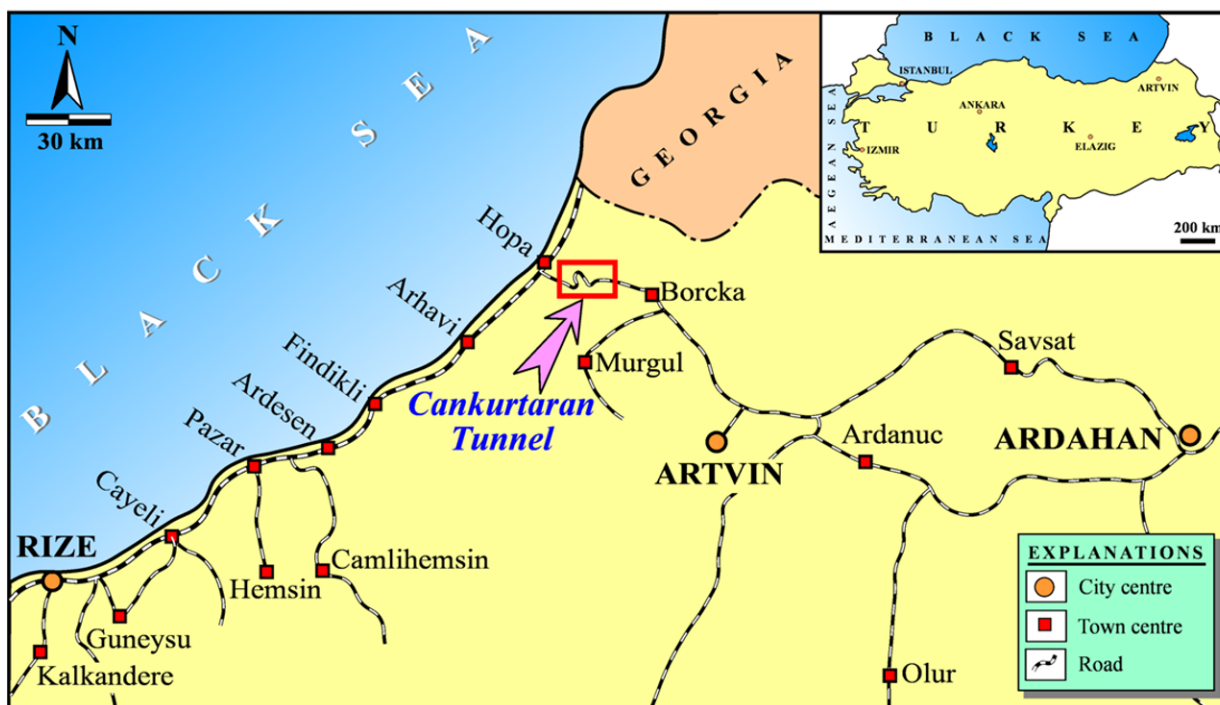


Figure 1 Location map of the study area.

Paleozoic to Quaternary.

In the study and surrounding area, geological units varying from old to young are the Late Cretaceous aged Subasi Ridge Formation, Late Cretaceous-Paleocene aged Cankurtaran Formation, Paleocene aged Senkaya Ridge Formation, Eocene aged Kabakoy Formation, and Quaternary aged alluvium (Capkinoglu 1981; Guven 1993; Kaya 2012; Kaya and Bulut 2013). A simplified geological map of the study and surrounding area is illustrated in Figure 3.

The Subasi Ridge Formation is a volcano-sedimentary deposit which is characterized by the andesitic pyroclastites and intercalations of limestone, marl, sandstone, tuff, and siltstone. This formation is commonly exposed in the entrance section of the Cankurtaran tunnel. The Cankurtaran Formation consists of limestone and marly-limestone conformably overlies the Subasi Ridge Formation. This unit crops out in the inner section of the tunnel. The Senkaya Ridge Formation is composed of marl with various colors (e.g. maroon, gray and yellow), limestone with partly red and gray laminate and intercalation of the claystone with thin and medium layers. The Eocene-aged Kabakoy Formation unconformably overlies the Senkaya Ridge Formation and crops out in the exit section of the tunnel. This formation

lithologically consists of basalt, andesite, and their pyroclastites. The Quaternary aged alluvium is the youngest unit in the area.

## 2 Engineering Geological Studies

Engineering geological properties of the andesitic tuffs were determined on the basis of the field observations/measurements and laboratory tests. The field studies were comprised of geological mapping, in-situ tests, geophysical and borehole investigations. The detailed information obtained from the engineering geological studies is given below;

### 2.1 Borehole investigations

Six investigation boreholes, (Figure 4) with a total length of 123 m were drilled (late-March) at the portal section immediately after the failure. These boreholes were used to identify the depth of the weathering zone, discontinuity properties, groundwater level, water pressure tests, and undisturbed sampling. The data obtained from the investigation boreholes indicated that the andesitic tuffs were composed of two different weathering zones. According to the ISRM (2007) suggested

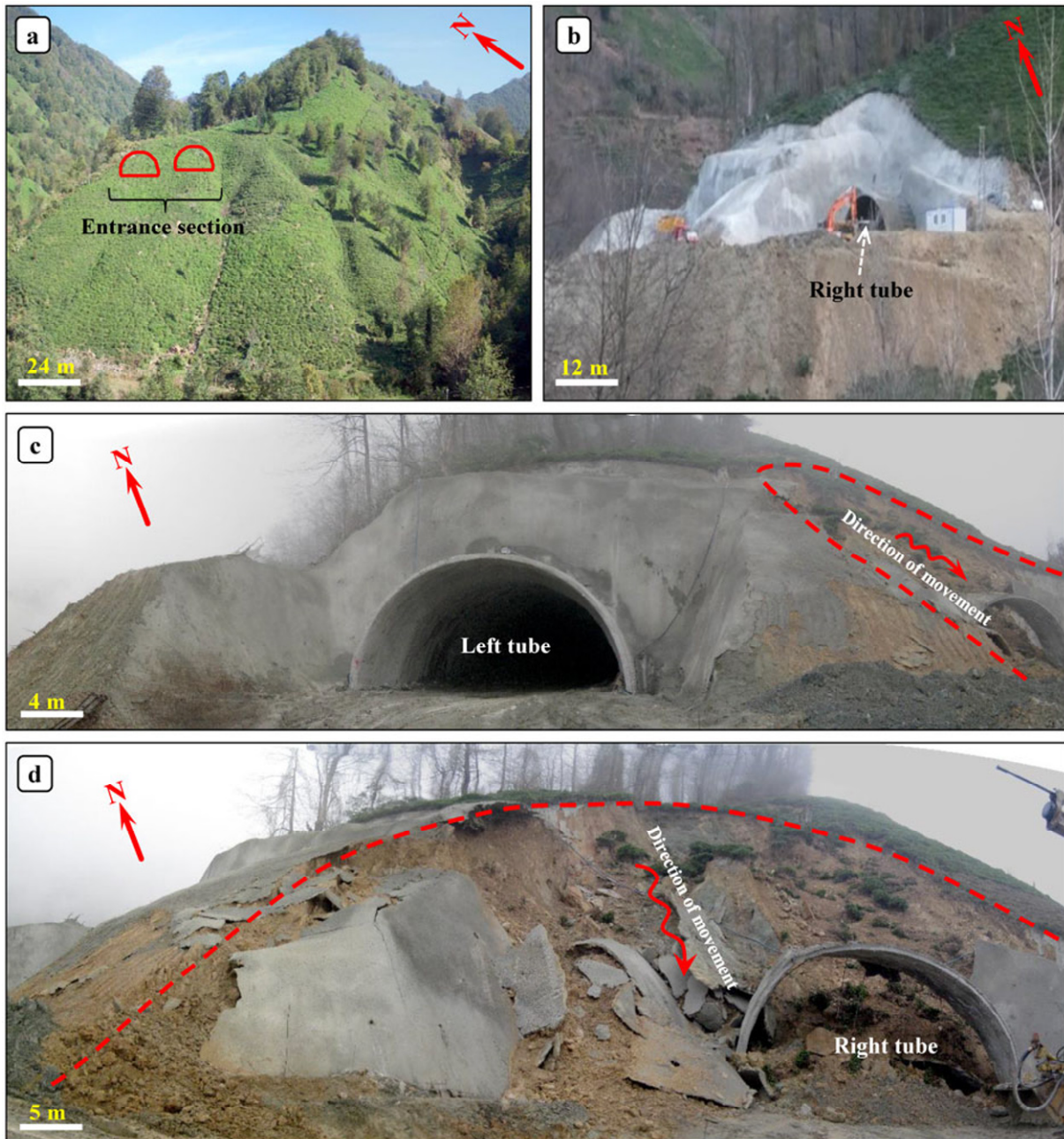


**Figure 2** (a) Pre- and (b) post-excitation view of the entrance portal and, field view of the (c) left and (d) right tubes after the failure.

method, the upper zone of the andesitic tuffs was classified as highly weathered with a ranging from 9 to 15 m and the fractured lower zone moderately weathered (Figure 5). The groundwater level ranged between 8.3 and 17.0 m. Further, the Rock Quality Designation (RQD) values of the moderately weathered andesitic tuff were identified from boreholes and classified as good rock mass (84%) based on the method suggested by Deere (1964).

The water pressure (Lugeon) tests (Lugeon

1933) were conducted in order to determine the permeability of the andesitic tuffs and, to gather information on the potential of the water inflow into the tunnel level. Values obtained from the Lugeon test indicated that the highly and moderately weathered andesitic tuffs were impermeable (0.12 L) and low permeable (2.86 L), respectively. Although the joints in the moderately weathered andesitic tuff are closely spaced, the low hydraulic conductivities can be explained by the filling of fractures with clays

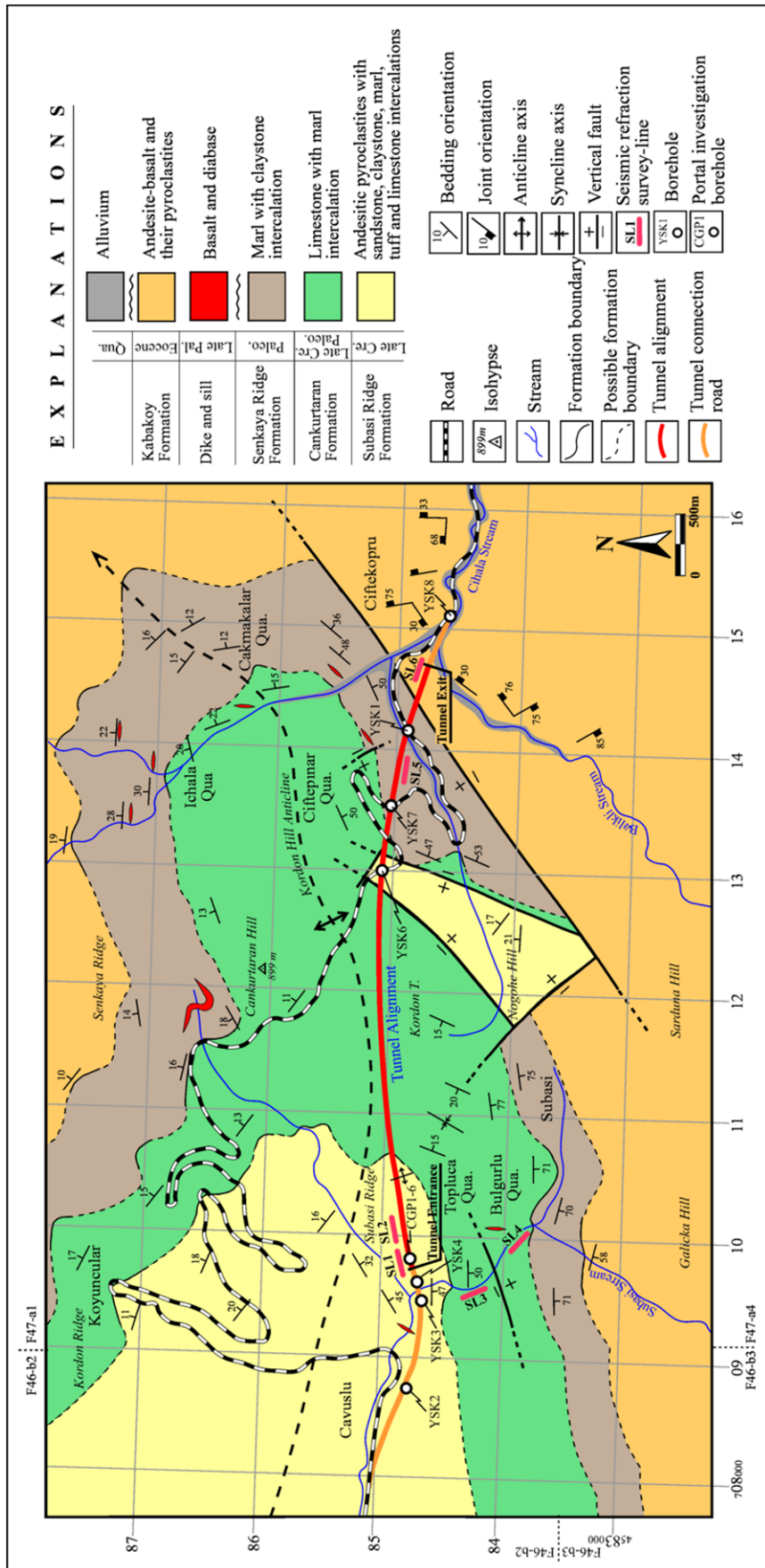


**Figure 3** Simplified geological map of the close vicinity of the study area (Modified from Capkinoglu 1981).

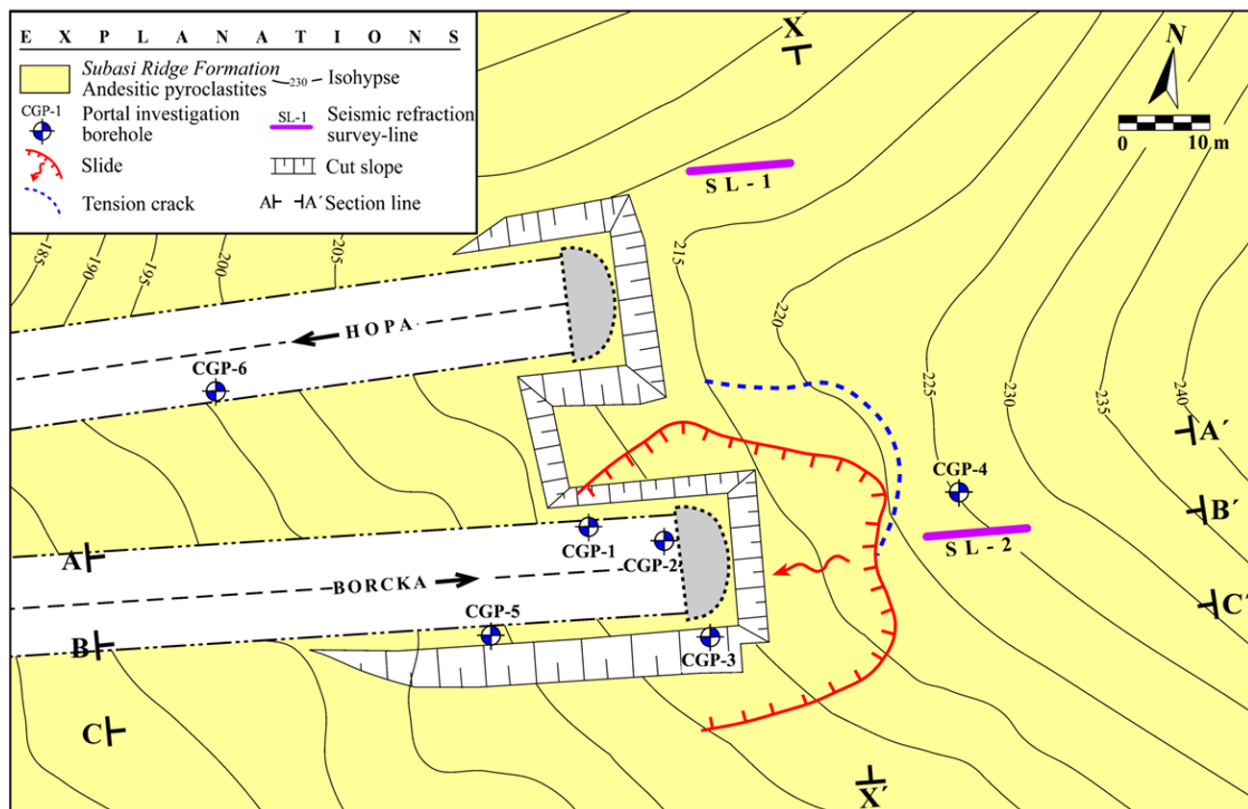


**Figure 4** Detailed geological map of the entrance portal section and its vicinity.

produced during weathering. These results show that the andesitic tuffs are generally dry and often show free water discharges such as leakages or drip.

The depth of boreholes, thickness of weathering zone, groundwater level, Lugeon test results, and RQD values are presented in [Table 1](#) and [Table 2](#).

## 2.2 Laboratory studies and back analyses

Due to the fact that the upper zone of the andesitic tuffs was highly weathered, the soil mechanics principle was applied in order to determine the unit weights and shear strength parameters according to [ASTM \(2009, 2011\)](#) standards ([Table 2](#)). Triaxial tests were performed under consolidated-undrained (CU) conditions on the undisturbed highly weathered tuff samples taken from the distressed zone of the slope, in order to identify the peak cohesion ( $c$ ) and peak internal friction angle ( $\phi$ ) values of the unfailed slope body. According to laboratory tests the peak  $c$  and  $\phi$  values were determined as 15 kPa and  $28^\circ$ , respectively. Furthermore, the residual shear strength parameters of the failed slope body were calculated by the help of limit equilibrium back analyses, using

the multiple solution method of [Sancio \(1981\)](#). Back analyses were carried out along the selected sections shown in [Figure 4](#) which were parallel to the movement direction (A-A', B-B' and C-C'). In this method, assuming the limit equilibrium condition (FOS=1), the  $c$  and  $\phi$  values are determined. Considering the circular shape of the failure surface, the back analyses were performed using the Bishop's simplified method ([Bishop 1955](#)) by means of Slide v6.0 ([Rocscience Inc. 2010](#)) software. The probabilistic analysis was applied to carry out the back analysis of two variables at the same time. Because the groundwater level passed through the moderately weathered andesitic tuff when the failure occurred, the highly weathered andesitic tuff was considered unsaturated in the back analyses. The residual cohesion and residual internal friction angle values at the sliding time were found to be 7 kPa and  $36^\circ$ , respectively from the back analyses ([Figure 6](#)).

Rock mechanics laboratory tests were performed on the rock cores taken from the moderately weathered andesitic tuff. The physico-mechanical and elastic properties, such as unit weight ( $\gamma$ ), point load strength index ( $I_{S(50)}$ ),

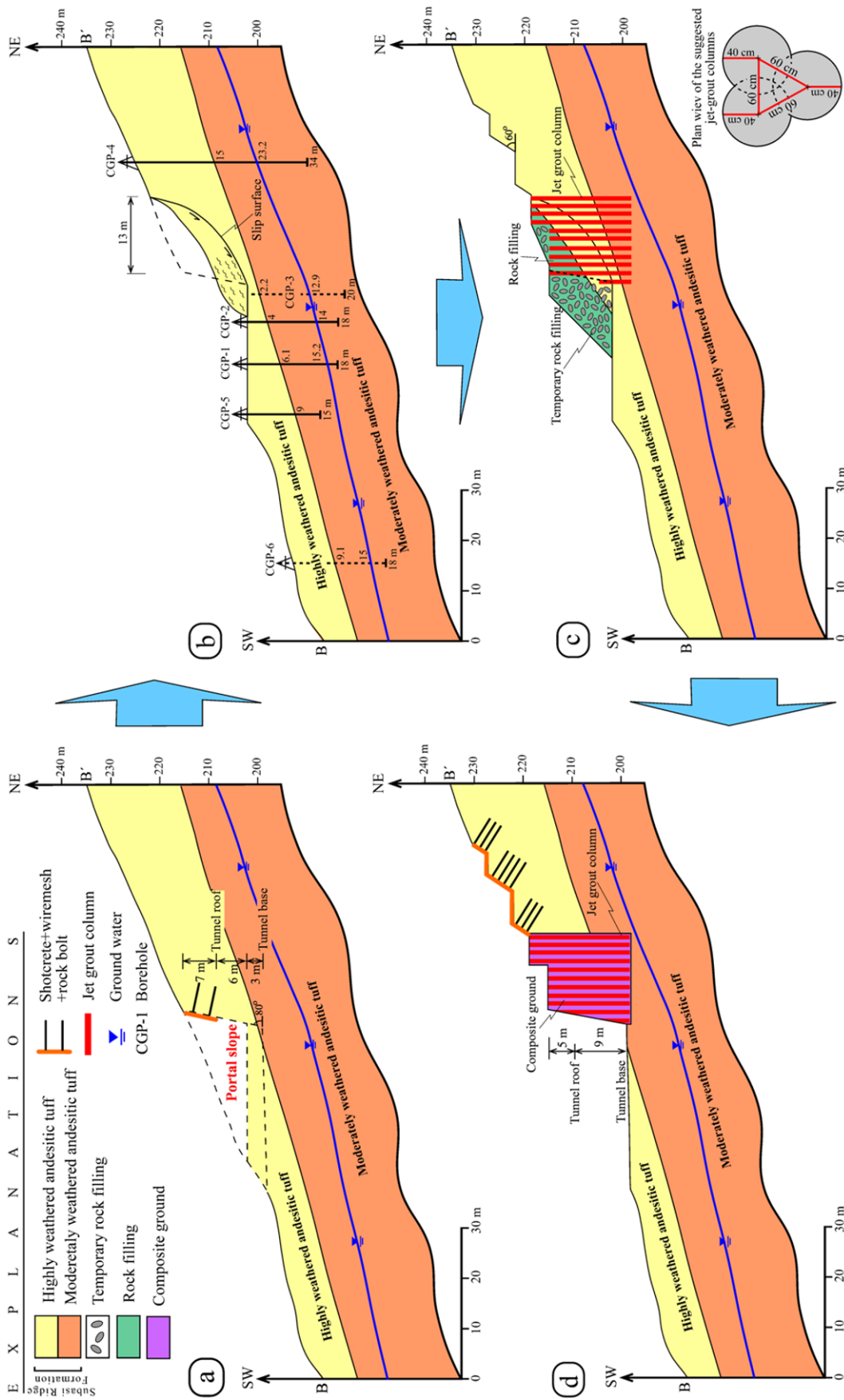


Figure 5 B-B' cross-sections showing the support installation steps along the failed portal slope.

uniaxial compressive strength ( $\sigma_{ci}$ ), Young's modulus ( $E_i$ ), and Poisson's ratio ( $\nu_i$ ) were determined according to [ISRM \(2007\)](#). [Table 2](#) shows the results of the laboratory tests.

### 2.3 Geotechnical properties of the joints in the moderately weathered andesitic tuff

The quantitative description of the joints in the moderately weathered andesitic tuff, such as orientation, spacing, persistence, infilling, roughness, aperture, and degree of weathering, were determined by the scan-line surveys and analyzing the cores according to the [ISRM \(2007\)](#) suggested method. These joints were described as being closely spaced with medium persistence, undulating, open, and moderately weathered ([Table 3](#)). In order to determine the main joint sets, a total of 715 joint measurements were taken and their orientations were processed by utilizing the Dips v5.1 ([Rocscience Inc. 2004](#)) software with

respect to equal-angle stereographic projection ([Figure 7](#)).

The Barton-Bandis failure criterion ([Barton and Bandis 1990](#)) was used to define the peak and residual shear strength parameters of the joint surfaces in the moderately weathered andesitic tuff. The suggested equations for the criterion are given below;

$$\phi_r = (\phi_b - 20) + 20(r/R) \tag{1}$$

$$\tau = \sigma_n \tan \left[ \phi_r + JRC \log \left( \frac{JCS}{\sigma_n} \right) \right] \tag{2}$$

where,  $\sigma_n$ : normal stress acting on the joint surface (MPa),  $\tau$ : shear strength of the joint surface (MPa),  $JCS$ : strength of the joint surface (MPa),  $JRC$ : joint roughness coefficient,  $\phi_r$ : residual friction angle,  $\phi_b$ : basic friction angle,  $R$ : Schmidt rebound value of the dry joint surface, and  $r$ : Schmidt rebound value of the wet joint surface.

This method was performed in two steps. Firstly, the deformation controlled direct shear tests proposed by [Mining Research Laboratories \(Canada\) \(1977\)](#) were carried out on the block samples, which had dimensions of 60x60x10 mm and the basic friction angle ( $\phi_b$ ) was determined to be 21° based on the drawn  $\tau$ - $\sigma$  graph ([Figure 8a](#)). The residual cohesion value ( $c_r$ ) was assumed to be 0 kPa in this criterion and the  $\phi_r$  value was calculated as 16° using [Eq.\(1\)](#). Secondly, the Barton-Bandis failure envelope was drawn using [Eq.\(2\)](#), by drawing the tangent representing the

**Table 1** Summary of the borehole data

Borehole no	Depth (m)	Elevation (m)	Thickness* (m)	Depth# (m)
CGP-1	18.0	207	6.1	15.2
CGP-2	18.0	209	4.0	14.0
CGP-3	20.0	208	2.2	12.9
CGP-4	35.0	225	15.0	23.2
CGP-5	15.0	204	9.0	-
CGP-6	18.0	196	9.1	18.0

**Notes:** Thickness\* refers to the thickness of the highly weathered andesitic tuff (m); Depth# refers to Ground water depth#.

**Table 2** Physico-mechanical and elastic properties of the highly and moderately weathered andesitic tuffs, RQD and Lugeon values

Property	Highly weathered andesitic tuff				Moderately weathered andesitic tuff			
	Min.	Max.	Ave.	SD.	Min.	Max.	Ave.	SD.
Rock quality designation (RQD, %)	-	-	-	-	59	93	84	12.59
Lugeon ( $L$ , l/min/m)	0	0.32	0.12	0.06	0.92	5.74	2.86	2.12
Point load strength index ( $Is(50)$ , MPa)	-	-	-	-	0.37	4.28	1.72	0.82
Uniaxial compressive strength ( $\sigma_{ci}$ , MPa)	-	-	-	-	5.47	63.38	25.47	12.41
Young's modulus ( $E_i$ , GPa)	-	-	-	-	11.09	44.57	28.85	15.02
Poisson's ratio ( $\nu_i$ )	-	-	-	-	0.18	0.23	0.20	0.11
Natural unit weight ( $\gamma_n$ , kN/m <sup>3</sup> )	17.34	18.56	17.67	1.18	23.12	24.65	24.26	2.02
Saturated unit weight ( $\gamma_s$ , kN/m <sup>3</sup> )	18.72	22.16	20.01	2.54	24.67	26.73	25.78	1.68
Cohesion ( $c$ , kPa) <sup>a</sup>	14	17	15	2.21	-	-	-	-
Internal friction angle ( $\phi_r$ ) <sup>a</sup>	26	33	28	4.13	-	-	-	-
Cohesion ( $c$ , kPa) <sup>b</sup>	-	-	7	-	-	-	-	-
Internal friction angle ( $\phi_r$ ) <sup>b</sup>	-	-	35	-	-	-	-	-

*Min.*: Minimum; *Max.*: Maximum; *Ave.*: Average; *SD.*: Standard deviation; <sup>a</sup> Values obtained from CU tests; <sup>b</sup> Values obtained from back analyses.



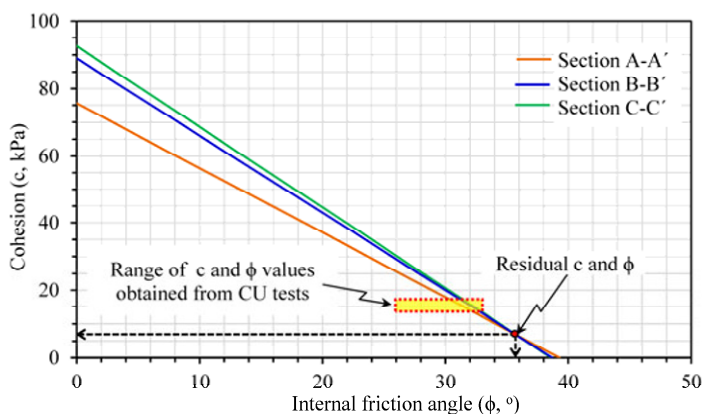


**Figure 6**  $c$ - $\phi$  graph of the highly weathered andesitic tuff showing the back analysis results.

**Table 3** Quantitative description of the joints in the moderately weathered andesitic tuff

Property	Value
Joint set number	3 + random
Joint set orientation	J1: 22/045 J2: 46/338 J3: 43/016
Joint spacing (cm)	(0.5-131) <sup>a</sup> 10.96
Persistence (m)	(0.2 -35) <sup>a</sup> 9.10
Aperture (mm)	(0-24.0) <sup>a</sup> 1.92
Infilling	<5 mm soft clay
Roughness	Rough, undulating
Weathering	Moderately weathered
Groundwater condition	Dripping

<sup>a</sup>: Average

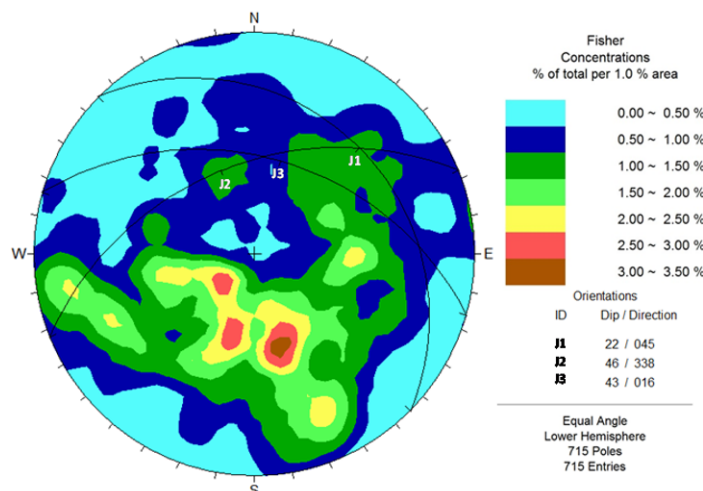


**Figure 7** Stereographic projection of the joint sets in the moderately weathered andesitic tuff.

Mohr-Coulomb failure envelope, the cohesion and peak friction angle of the joint surfaces were determined as 18 kPa and 32°, respectively (Figure 8b). These values were later used in the numerical

analyses. The parameters used in the Barton-Bandis failure criterion and results are given in Table 4.

### 2.4 Rock mass properties of the andesitic tuffs

In order to determine the deformation modulus ( $E_m$ ) of the highly and moderately weathered andesitic tuffs, a total of 15 pressuremeter tests were conducted in the CGP 2 and 4 boreholes according to the procedures suggested by Menard (1975) and ASTM (2000). The pressuremeter test was developed by Menard (1956) for in-situ evaluation which can provide the stress and deformation relationships for a particular ground condition. Eq.(3), as suggested by Menard (1975), was used in the calculation of the deformation modulus.

The geophysical studies were performed using the seismic refraction method in the two lines (Figure 4) using a 12-channel Geometrics ES3000 model seismograph to determine the dynamic Poisson’s ratio ( $\nu_m$ ) of the highly and moderately weathered andesitic tuffs. Seismic refraction is a geophysical exploration method which uses the basis of seismology to estimate the properties of the earth’s subsurface using the refracted seismic waves. When performing the seismic studies primary-wave ( $V_p$ ) and secondary-wave ( $V_s$ ) velocities were determined for andesitic tuffs studied. The dynamic Poisson’s ratio values were calculated using Eq.(4) proposed by Bowles (1988).

The Geological Strength Index (GSI) value of the moderately weathered andesitic tuff was defined using Eq.(5) suggested by Hoek et al. (2013) and it was classified as a blocky rock mass in accordance with the last version of the quantitative GSI chart. The rock mass parameters such as Hoek-Brown constants ( $m_b$ ,  $s$ ,  $a$ ), uniaxial compressive strength ( $\sigma_{cm}$ ), cohesion ( $c$ ), and friction angle ( $\phi$ ) are necessary inputs for numerical analyses. In order to determine these parameters for moderately weathered andesitic tuff,

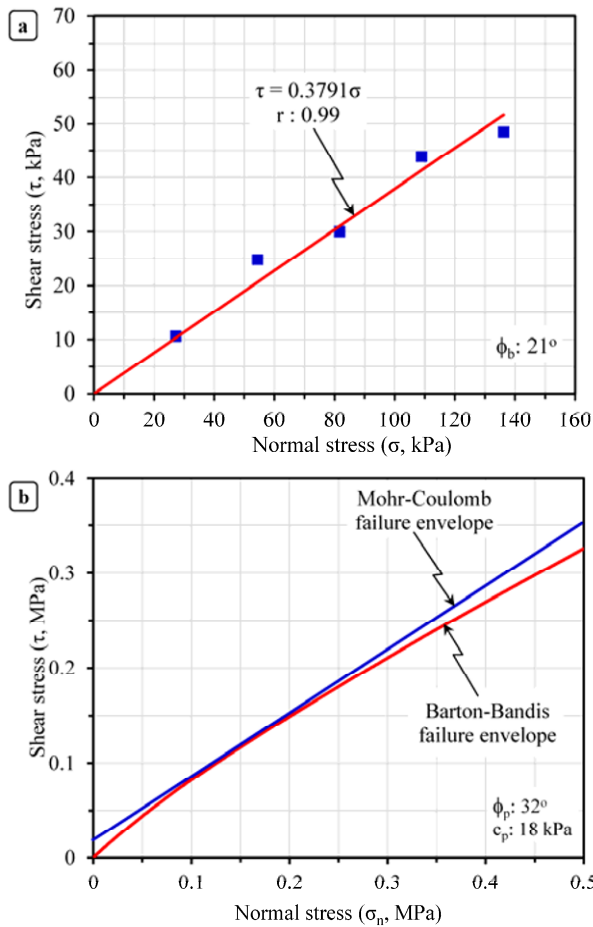


**Figure 8**  $\sigma$ - $\tau$  graphs for (a)  $\phi_b$  and (b)  $\phi_p$ - $c_p$  values of the joints in the moderately weathered andesitic tuff.

**Table 4** Parameters used in the Barton-Bandis failure criterion and the shear strength parameters of the joints in the moderately weathered andesitic tuff

Parameter	Value
Basic friction angle ( $\phi_b$ , °)	21
Dry Schmidt rebound ( $R$ )	38
Wet Schmidt rebound ( $r$ )	29
Residual friction angle ( $\phi_r$ , °)	16
Residual cohesion ( $c_r$ , kPa)	0
Joint compressive strength ( $JCS$ , MPa)	37
Joint roughness coefficient ( $JRC$ )	9
Peak cohesion ( $c_p$ , kPa)	18
Peak friction angle ( $\phi_p$ , °)	32

the Hoek-Brown failure criterion proposed by Hoek et al. (2002) was used and rock mass parameters were calculated using Eqs.(6)-(11).

To determine the post-peak behavior of the moderately weathered andesitic tuff, the method proposed by Cai et al. (2007) was utilized. The

residual Geological Strength Index ( $GSI_r$ ) and residual Hoek-Brown constants ( $m_{br}$ ,  $s_r$ ,  $a_r$ ) were calculated using Eqs.(12)-(15).

Since the mechanical excavation will be applied, a disturbance factor ( $D$ ) value of zero was considered. The  $m_i$  constant of the moderately weathered andesitic tuff was defined with the help of Roclab v1.0 (Rocscience Inc. 2002) software and assumed to be 13.

The estimated rock mass parameters for each zone and equations used in the calculations are given in Table 5.

### 3 Slope Stability Analyses

In relevant literature limit equilibrium, empirical, stress analysis, physical, and numerical methods are generally used to determine the stability of the rock and soil slopes (e.g. Fellenius 1936; Janbu 1954; Bishop and Morgenstern 1960; Lowe and Karafiath 1959; Morgenstern and Price 1967; Spencer 1967; USCE 1970; Sarma 1973; Fell et al. 1996; Shukra and Baker 2003; Hart et al. 2008; Karaman et al. 2013). In numerical stability analyses analytic element method (AEM), finite difference method (FDM), boundary element method (BEM), discrete element method (DEM), and finite element method (FEM) based softwares are used for the reflection of rock mass behavior. The major advantage of using numerical methods, rather than conventional limit equilibrium method, is that the joint properties of the discontinuous rock masses can be modelled. Since finite element method (FEM) considers the geometry of slope, forces acting on a slope forming material and physico-mechanical/ elastic parameters, it has become one of the most preferred methods in geotechnical projects by designers. In order to find out the factor of safety (FOS) in accordance with the conventional limit equilibrium methods in conception, Griffiths and Lane (1999) combined the finite element method (FEM) with the shear strength reduction technique (SSR) to determine the FOS value. In the FEM-SSR method, the factor of safety (FOS) is symbolized by the Strength Reduction Factor (SRF). The SRF value is the ratio between the actual and the model strength at the stability limit. The main advantage of the SSR method is that there is no need to the primary

guess at determination of critical failure surface. Due to the rapid advances in computer systems, FEM-SSR method is increasingly used today (e.g. Matsui and Sam 1992; Shukra and Baker 2003; Hammah et al. 2006; Li 2007; Karaman 2013; Kaya et al. 2015; Kaya 2016).

In this study, the geometry of the portal slope was modeled with a FEM based computer package called as Phase<sup>2</sup> v8.0 (Rocscience Inc. 2011). Phase<sup>2</sup>, which allows 2-D plane strain modelling, is powerful and flexible software that has the Shear Strength Reduction (SSR) method combined with

the FEM and interpretation modules (FEM-SSR). The slope profile along the B-B' section is drawn incorporating field information and the finite element analyses have been performed along this profile section. In the analyses models, finer zoning was applied and a total of 500 uniform typed and six-nodded triangular finite elements were chosen in the mesh. The solutions were made under gravitational loading (gravitational stress distribution throughout the slope). By using the actual ground surface option, the ground surface above every finite-element was determined and the

**Table 5** Calculated rock mass parameters of the highly and moderately weathered andesitic tuffs

Researcher	Equation	Note	Equation number	Highly weathered andesitic tuff	Moderately weathered andesitic tuff
Menard (1975)	$E_m = (1 + \nu) 2V \left( \frac{\Delta P}{\Delta V} \right)$	MPa	(3)	16.37	2461.95
Bowles (1988)	$\nu_m = \frac{V_p^2 - 2V_s^2}{2(V_p^2 - V_s^2)}$		(4)	0.41	0.23
Hoek et al. (2013)	$GSI = 1.5 JCond_{89} + RQD / 2$	RQD: 84 % JCond <sub>89</sub> : 13	(5)	-	61.5
Hoek et al. (2002)	$m_b = m_t e^{\left( \frac{GSI-100}{28-14D} \right)}$	m <sub>i</sub> : 13 D: 0	(6)	-	3.29
	$s = e^{\left( \frac{GSI-100}{9-3D} \right)}$	GSI: 61.5	(7)	-	0.0139
	$a = \frac{1}{2} + \frac{1}{6} \left( e^{-GSI/15} - e^{-20/3} \right)$		(8)	-	0.503
	$\sigma_{cm} = \sigma_{ci} \cdot \frac{(m_b + 4s - a(m_b - 8s))(m_b / 4 + s)^{a-1}}{2(1+a)(2+a)}$	MPa	(9)	-	6.53
Hoek et al. (2002)	$c_m = \frac{\sigma_{ci} \left[ (1+2a)s + (1-a)m_b \sigma'_{3n} \right] (s + m_b \sigma'_{3n})^{a-1}}{(1+a)(2+a) \sqrt{1 + \left[ 6am_b (s + m_b \sigma'_{3n})^{a-1} \right] / \left[ (1+a)(2+a) \right]}}$	kPa	(10)	-	1641 <sup>a</sup> 925 <sup>b</sup>
	$\phi_m = \sin^{-1} \left[ \frac{6am_b (s + m_b \sigma'_{3n})^{a-1}}{2(1+a)(2+a) + 6am_b (s + m_b \sigma'_{3n})^{a-1}} \right]$	degree	(11)	-	36 <sup>a</sup> 26 <sup>b</sup>
	$GSI_r = GSI e^{-0.0134GSI}$		(12)	-	27
Cai et al. (2007)	$m_{br} = m_t e^{\left( \frac{GSIr-100}{28} \right)}$		(13)	-	0.96
	$s_r = e^{\left( \frac{GSIr-100}{9} \right)}$		(14)	-	0.00030
	$a_r = \frac{1}{2} + \frac{1}{6} \left( e^{-GSIr/15} - e^{-20/3} \right)$		(15)	-	0.527

V: Sum of the initial volume of the measuring cell and mean additional volume injected into the measurement probe; ΔV and ΔP: Change of volume and change in pressure during the pseudo elastic phase; V<sub>p</sub>: Primary-wave velocity (m/sec), V<sub>s</sub>: Secondary-wave velocity (m/sec); JCond<sub>89</sub>: Joint condition rating defined by Bieniawski (1989); a: Peak values and b: Residual values necessary input for tunnel analysis calculated by Cai et al. (2007).

vertical stress in the element based on the weight of material above it was defined. In order to prevent displacements occurring at the bottom and along the vertical boundary of the model, the vertical and horizontal displacement was set to zero. Free boundary condition was applied to the ground surface. The horizontal stress ratio was entered as 1, representing hydrostatic initial stresses (horizontal stress = vertical stress). After introducing the external boundary mesh type, field stress and the material properties of the weathered andesitic tuffs that comprise the slope were defined using the geotechnical parameters given in [Table 2](#) and [Table 5](#). The analyses models were divided into two separate zones. The highly weathered upper zone of the andesitic tuff was assumed to be a continuous rock mass and the fractured lower zone was assumed to be a discontinuous rock mass. Through the development of special elements (joint elements sometimes also known as interface elements), the continuum-based FEM can also be applied to the modelling of discontinuous rock masses ([Goodman et al. 1968](#); [Ghaboussi et al. 1973](#); [Beer 1985](#)). These elements can have either zero thickness or a thin, finite thickness. They can assume linear elastic behaviour or plastic response when stresses exceed the strengths of discontinuities ([Hammah et al. 2008](#)). In FEM-SSR method, discontinuity is represented as a joint element, which provides relaxed connectivity between two adjacent rock walls in contact. A joint is assigned strength and stiffness properties. The properties of the joint sets (orientation, spacing, length, and shear strength parameters) located in the moderately weathered andesitic tuff ([Table 3](#) and [Table 4](#)) were inserted into the analyses models as the joint network and the ends of all joints in a network were assumed to be closed. Normal and shear stiffness parameters of the joints were estimated using the method suggested by [Barton \(1972\)](#) based on the deformation properties of the rock mass and the intact rock. Another important parameter in the analysis was the groundwater. In order to define the groundwater, a piezometric line was drawn above the external boundary based on information obtained from borehole investigations and changes in the total stress were investigated. The auto Hu option was used to estimate the pore pressures based on the inclination of the ground water surface. Since the

groundwater level passed through the moderately weathered andesitic tuff (considered as fractured rock mass) when the failure occurred, the effect of negative pore pressure (referred as matric suction) occurring above the water table on the highly weathered andesitic tuff (considered as soil) was not considered in the analyses. The Mohr-Coulomb failure criterion suggested by [Mohr \(1900\)](#) was used in the FEM-SSR analyses to describe the properties of the rock masses and joints in order to get more realistic results and to model the zones in a single failure criterion method. Because the elastic-perfectly plastic (EPP) model best replicates the limit equilibrium analysis, both highly and moderately weathered andesitic tuffs were considered to be EPP material. To understand the occurrence mechanism of the failure at the right tube portal slope and to determine remedial measures, FEM-SSR analyses were carried out in three stages under static and dynamic conditions as follows.

### 3.1 Slope stability analysis for the pre-excavation and post-excavation cases

In order to investigate the stability of the slope having a natural topographical geometry (before the excavation), the slope profile given in [Figure 5a](#) was modeled in the Phase<sup>2</sup> software. The unsaturated highly weathered andesitic tuff, which comprises the upper zone of the slope was defined using the shear strength parameters ( $c= 7$  kPa and  $\phi= 35^\circ$ ) obtained from back analyses. In order to identify the lower zone of the slope,  $c= 1641$  kPa and  $\phi= 36^\circ$  values for the moderately weathered andesitic tuff and  $c= 18$  kPa and  $\phi= 32^\circ$  values for the joints were utilized.

A piezometric line representing the groundwater table passing through the lower zone was drawn in the analysis model. According to the static analysis performed for the pre-excavation case, the SRF value was determined as 1.96 and a composite (circular+linear) shaped critical slip surface was located in the weathering contact zone as expected ([Figure 9a](#)). Consequently, since the calculated SRF value was greater than the limit equilibrium condition (FOS = 1), any failures were not expected to occur during pre-excavation case and the slope was stable under static conditions. Based on the field observations performed before

the excavation work, any tension cracks or deformations were not detected on the ground (Figure 2a). Thus, the stability analysis result shows a strong correlation with the real-field situation.

In the post-excavation stage, a portal excavation with an approximate height of 13 m (Figure 5a) was applied into the pre-excavation analysis model and, 10 cm shotcrete with one layer wiremesh and 6 m long rock bolts with  $2.0 \times 2.0$  m spacing were installed same as the actual situation. In order to identify the unfailed slope body, the same shear strength parameters and ground water conditions used in the pre-excavation analysis model were taken into account. The stability properties of the unsupported and supported slope were investigated respectively. Because the portal failure was not triggered by a seismic activity, the numerical analyses were performed under the static conditions to understand the occurrence mechanism of the failure. The characteristics and pattern of the installed initial support units for the post-excavation case are presented in Table 6 and Table 7. As a result of the numerical analyses performed for the post-excavation case, the SRF values of the unsupported and supported cut slope were found to be 0.63 and 0.83, correspondingly (Figure 9b) and it was concluded that both values were smaller than the limit equilibrium condition (FOS=1). As can be seen from Figure 9b, a circular shaped stress concentration was developed 13 m behind the slope face and exhibited a very good match with the original failure surface. The results of the FEM-SSR analyses show a close agreement with the actual field observations (Figure 5b) and, prove that the use of back analyses results in stability assessments seem to be reliable. It was clearly understood that weathering considerably reduced the resistance of the andesitic tuffs against sliding and stress relief during the excavation played an important role in this failure and the applied initial support units were not sufficient to make slope stable. Since the failure occurred end of the rainy season (late-March), no significant groundwater existed within the failed body and no surface drainage was observed in the site (Figures 2a and 2b). However, it was considered that the percolation of surface water into the highly weathered andesitic tuffs probably played an additional role in sliding that resulted in a decrease

in the shear strength. The special precautions proposed to prevent the effects of this failure and to stabilize the portal slope are discussed in Section 3.2.

### 3.2 Remedial design consideration

In the final stage, the selected remediation for this failure is discussed. These measures are essential for the safety and the cost of the engineering projects. In landslide remediation applications, there are various methods which include bridging, buttressing, flattening, reinforcement, rerouting, retaining walls, soil hardening, surface and subsurface drainage, surface slope protection, thermal treatment, unloading, and vegetation (Turner and Schuster 1996; Abramson et al. 2001; Fahimifar et al. 2013). However, tunnel portal failures require special design measures in the stabilization process since the stability of portal slopes and openings are quite important in tunneling projects. Because the rock retaining wall with the jet grout columns to be the most economic and reliable reinforcement type to make the both portal slope and tunnel stable (e.g. Guatteri et al. 1988; Pelizza and Peila 1993; Brill et al. 2003) thus, it was chosen in order to prevent any effect of the tunnel portal failure. In this study, the application of the recommended remedial measures is carried out in three steps. In the first step, the front portion of the slide material will be removed from the right tube and a rock retaining wall will be constructed (Figure 5c). In the second step, to improve the rock filling and slide materials, the 80 cm diameter crossed jet grout columns will be placed deep into the tunnel base level and a composite ground will be created (Figure 5c). In the final step, in addition to the jet grout application, the upper part of the right tube will be benched and reinforced with shotcrete, wiremesh, and rock bolts for the long-term stability (Figure 5d). Considering the information gained from the trial jet grout columns applied in the study area by Turkish General Directorate of Highways (KGM), the shear strength parameters ( $c$  and  $\phi$ ) and unit weight ( $\gamma$ ) of the composite ground were inserted into the model as 490 kPa,  $29^\circ$  and, 25 kN/m<sup>3</sup>, respectively. Characteristics of the chosen support units and their pattern used in the FEM-SSR analyses are given in Table 6 and Table 7.

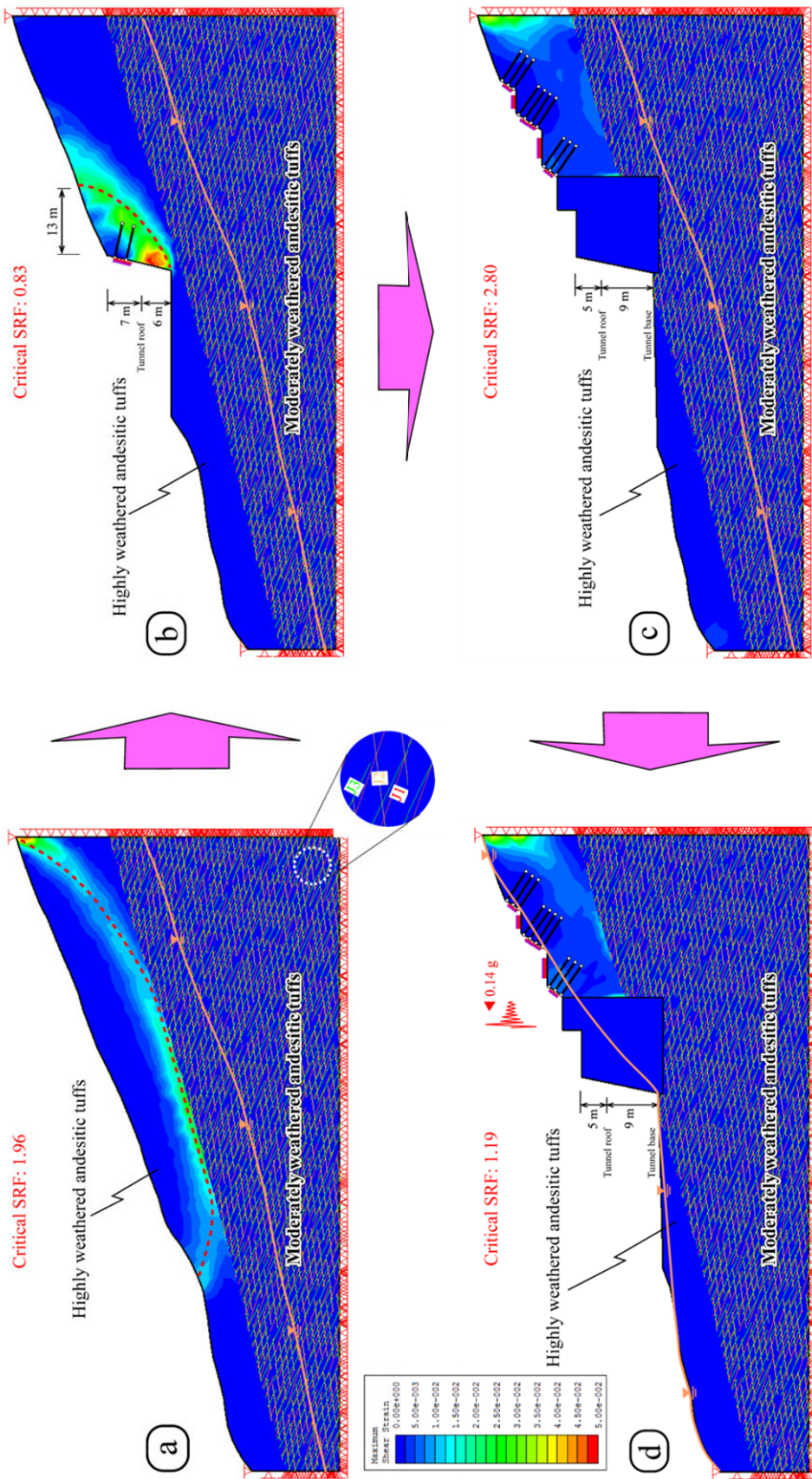


**Table 6** Characteristics of the support units used in the numerical analyses (KGM 2013)

Properties	Shotcrete	Wiremesh	Rock bolt	Steel rib
Young's modulus ( $E$ , GPa)	20	200	200	200
Poisson's ratio ( $\nu$ )	0.2	0.35	-	0.35
Peak uniaxial compressive strength ( $\sigma_{cp}$ , MPa)	20	400	-	400
Residual uniaxial compressive strength ( $\sigma_{cr}$ , MPa)	3.5	-	-	-
Peak tensile strength ( $\sigma_{tp}$ , MPa)	3.1	500	-	500
Residual tensile strength ( $\sigma_{tr}$ , MPa)	0	-	-	-
Peak load (MN)	-	-	0.25	-
Residual load (MN)	-	-	0.025	-
Type	-	Ø6.5 mm, 150×150 mm	Ø28 mm fully bonded	I-beam 160 cm × 42.6 kg/m

**Table 7** Pattern of the applied and proposed support units for the portal slope

Support unit	Applied support design for the portal slope	Proposed support design for the upper benches
Shotcrete	Thickness: 10 cm	Thickness: 10 cm
Wiremesh	Type: Ø6.5 mm one layer; Mesh spacing: 150×150 mm	Type: Ø6.5 mm one layer; Mesh spacing: 150×150 mm
Rock bolt	Type: Ø28 mm fully bonded; Length: 6.0 m; Spacing: 2.0×2.0 m	Type: Ø28 mm fully bonded Length: 6.0 m; Spacing: 1.25×1.25 m

The performance of the proposed remediation design was controlled in two steps, static short-term and dynamic long-term stability, using Mohr-Coulomb failure criterion. As previously mentioned, the validity of the shear strength parameters had already been verified in the analyses of the pre- and post-excavation stages and the results compared well with the observed actual field situation. Therefore, in the first step, the static short-term stability of the slope design was investigated using the shear strength parameters utilized in the pre- and post-excavation cases (Figure 9c). The result of the slope stability analysis showed that the proposed measure was sufficient to stabilize the failure which led to a SRF value of 2.80 under static conditions (Figure 9c). For the stability of slopes, a FOS value that is equal or greater than 1.5 is generally preferred for static conditions and a FOS value of 1.1 is required with earthquake effect (KGM 2013). The obtained SRF value is considered to be high enough for the short-term slope stability with the conservative parameters used.

In the second step, the long-term stability of the proposed slope design under fully saturated conditions and earthquake effect (pseudo-static stability analysis) was investigated. The information determined from field/laboratory experiments and estimations were employed in the analyses by taking the worst conditions into account. Because no water drainage took place during the shearing in CU tests, the saturated highly weathered andesitic tuff was characterized

by the shear strength parameters ( $c= 15$  kPa and  $\phi= 28^\circ$ ) obtained from CU tests. In order to identify the lower zone of the slope, the shear strength parameters of the moderately weathered andesitic tuff ( $c= 1641$  kPa and  $\phi= 36^\circ$ ) and the joints ( $c= 18$  kPa and  $\phi= 32^\circ$ ) were used.

The external factors (i.e., groundwater, earthquake, weathering degree and human activities) that affect slope stability induce the damages. During the earthquake, while the rock mass strength and the shear strength of joints are progressively reduced, the deformation is increased and hence, so is the limit above which further damage can be induced. The Black Sea Fault beneath the sea which is approximately 17 km away from the entrance portal of the Cankurtaran tunnel was considered in seismic load determination. An earthquake with a magnitude of  $M_w=6.0$  was considered in the calculation of the design ground motion parameter. Taking into account the distance of the Black Sea Fault and ground type, the peak ground acceleration (PGA) value was calculated as 0.14 g using the Ulusay et al. (2004) attenuation relationship suggested for Turkey. Therefore, a seismic acceleration coefficient of 0.14 g was employed for the long-term stability analysis of the slope, as a conservative approach.

According to the dynamic long-term stability analysis result, a SRF value of 1.19 was achieved if the slope was fully saturated and under the effect of earthquake (Figure 9d). This result indicated that the obtained SRF value was greater than the

acceptable FOS value of 1.1 and utilization of proposed measure at the tunnel portal revealed that the failure could be stabilized dynamically. As a result, it is clearly understood that this remediation design is sufficient for the short- and long-term stability in these kinds of problematic grounds.

In tunneling projects, not only the stability of portal slopes but also the stability of openings in portal sections has to be further investigated. The detailed information obtained from geotechnical studies for tunnel stability is given in Section 4.

#### 4 Tunnel Support Design of the Entrance Portal Section

In order to conduct the empirical tunnel support design and to characterize the weathered andesitic tuffs crop out at the entrance portal section of Cankurtaran tunnel, most commonly utilized rock mass classification systems such as Rock Mass Rating (RMR), Rock Mass Quality (Q) and New Austrian Tunneling Method (NATM) were employed using the data obtained from field studies, boreholes, and laboratory tests.

According to the RMR (Bieniawski 1989) system, the moderately and highly weathered andesitic tuffs were classified as 28/poor and 16/very poor, respectively. In terms of the Q system (Barton et al. 1974), the moderately weathered andesitic tuff was classified as 0.35/very poor and as 0.017/extremely poor for highly weathered andesitic tuff. Considering the Ö-NORM B2203

(1994) standard related to NATM system, the moderately weathered andesitic tuff was classified as B3/rolling and as C2/squeezing for the highly weathered andesitic tuff (Table 8).

The entrance portal section of tunnel will be constructed using the conventional mechanical excavation method and the planned excavation section of double tube tunnel is modified horse-shoe with 12 m width and 9 m height. The planned construction characteristics include construction phase, round length, stand-up time and support time are presented in Table 8. Because the RMR system suggests support elements only for horse-shoe shaped span of 10 m, vertical stress lower than 25 MPa and drilling-blasting construction, the support design therefore was obtained using the support chart suggested by Barton (2002) based on the Q values (Table 8).

To determine the induced stresses, deformations, and developed plastic zones around the tunnel and to verify the results of the Q system, the FEM based Phase<sup>2</sup> software was used in the numerical tunnel analyses. Characteristics of the chosen support units and their pattern employed in the FEM analyses are given in Table 6 and Table 8. In order to simulate the excavation boundary of double-tubed tunnel including composite ground, the finite element model was generated along the X-X' section (Figure 4). According to construction procedure of the NATM specification suggested by KGM (2013), two-phased excavation model consists of top heading and bench was applied to the analysis model. Same failure criterion,

**Table 8** Rock mass classes according to the Rock Mass Rating (RMR), Rock Mass Quality (Q) and New Austrian Tunneling Method (NATM) systems and empirical tunnel support units

Classification system		Highly weathered andesitic tuff	Moderately weathered andesitic tuff
RMR	Basic RMR value	16.0	46.4
	Adjusted RMR value	16.0	28.0
	Classification	Very poor	Poor
Q	Value	0.017	0.35
	Classification	Extremely poor	Very poor
NATM	Class	C2	B3
	Classification	Squeezing	Rolling
Support	Left tube	Systematic rock bolts 4 m long, spaced 1.0-1.2 m and ≥250 mm thick reinforced shotcrete (Sfr+B) with two layer wiremesh and steel ribs (RRS) in crown and wall	
	Right tube	100 mm thick reinforced shotcrete (Sfr+B) with one layer wiremesh in crown and wall	
Excavation method		Mechanical excavation	
Construction phase		Top heading and bench	
Round length		0.5-1.0 m advance in top heading and 1.5 m in bench	
Stand-up time		Immediate collapse	
Support time		Install support concurrently with excavation	



material/joint properties (peak and residual shear strength values) and boundary types including external boundary, mesh type, field stress, and groundwater conditions utilized in the slope stability analyses were considered in the tunnel analyses models (Figure 10a). The post-peak behavior of the moderately weathered andesitic tuff was characterized using the residual shear strength parameters given in Table 5. To determine the plastic zones and yielded elements in the vicinity of the tunnel, the FEM analyses were performed for the unsupported and supported cases in three steps.

In the first step, following the examination of in-situ stress distributions, the yielded points, principal stress distributions, and induced displacements developed around the tunnel excavations before the support installation (unsupported case) were inspected. Further, the maximum thickness of the plastic zones and total displacements were examined. According to Lugeon test the highly and moderately weathered andesitic tuffs are generally impermeable (0.12 L) and low permeable (2.86 L), respectively. These properties cause the water inflow into the tunnel level such as permanent leakages or drip in rainy seasons. Because the highest rate of precipitation for the site was observed only in the spring, the portal stabilization and excavation studies will be carried out in dry season to provide a safe work environment. According to FEM analysis results of the planned excavation scenario, the maximum total displacement emerged in the highly weathered zone and maximum stress concentration developed only at the top of the excavation in left tube (Figure 10b and Table 9). The elements undergoing yielding and extent of the plastic zones show that there would be a stability problem in the left tube if it is not supported. However, the stability problem is not expected to occur in the right tube excavated in composite ground. Therefore, the support elements have to be installed immediately after excavations in left tube without allowing the deformations.

In the second step, the performance of the proposed empirical support design was investigated using the same analysis model. To be on the safe side, the support system proposed for highly weathered andesitic tuff was applied to the left tube and 100 mm shotcrete was applied to the right tube. The characteristics of the support

elements and its pattern used in the FEM analysis are given in Table 6 and Table 8. Changes in the thickness of the plastic zones and the maximum total displacements after the support applications were analyzed and the results were also compared. After the installation of support elements, it was found that the empirical support design was sufficient to eliminate the stability problem in the left tube and the maximum thickness of the plastic zones were decreased from 11.69 m to zero (Figure 10c and Table 9).

In the final step, long-term dynamic performance of the support elements were investigated using the same analysis model considering the appropriate parameters (fully saturated and earthquake effect). A seismic acceleration coefficient of 0.14 g was employed in the FEM analysis. According to the analysis, the support systems reduced the maximum thicknesses of plastic zone value from 11.69 m to 1.94 m in the left tube and there was no considerable plastic zone in the crown and walls. Therefore, it was concluded that there would not be stability problems for the tunnel driven in entrance portal section and the support recommendations gave satisfactory results for the long-term dynamic conditions (Figure 10d and Table 9). Based on the long-term analysis of the tunnel, remedial measures are suggested with design guidelines to provide the stability of tunnel portal.

## 5 Conclusions

A portal failure occurred at the entrance section of the Cankurtaran tunnel after slope excavation in highly weathered andesitic tuffs. Therefore, a detailed engineering geological investigation including surface, subsurface, laboratory studies and FEM based slope and tunnel stability analyses were performed. The outcomes can be summarized as follows:

(1) The numerical stability analysis for the pre-excavation case with a SRF value of 1.96 demonstrated that circular or composite failures are not possible to occur in the slope having natural topographical geometry. However, circular toe failure is expected in post-excavation case of the portal slope with a SRF value of 0.83 even supports with shotcrete, wiremesh and bolts.

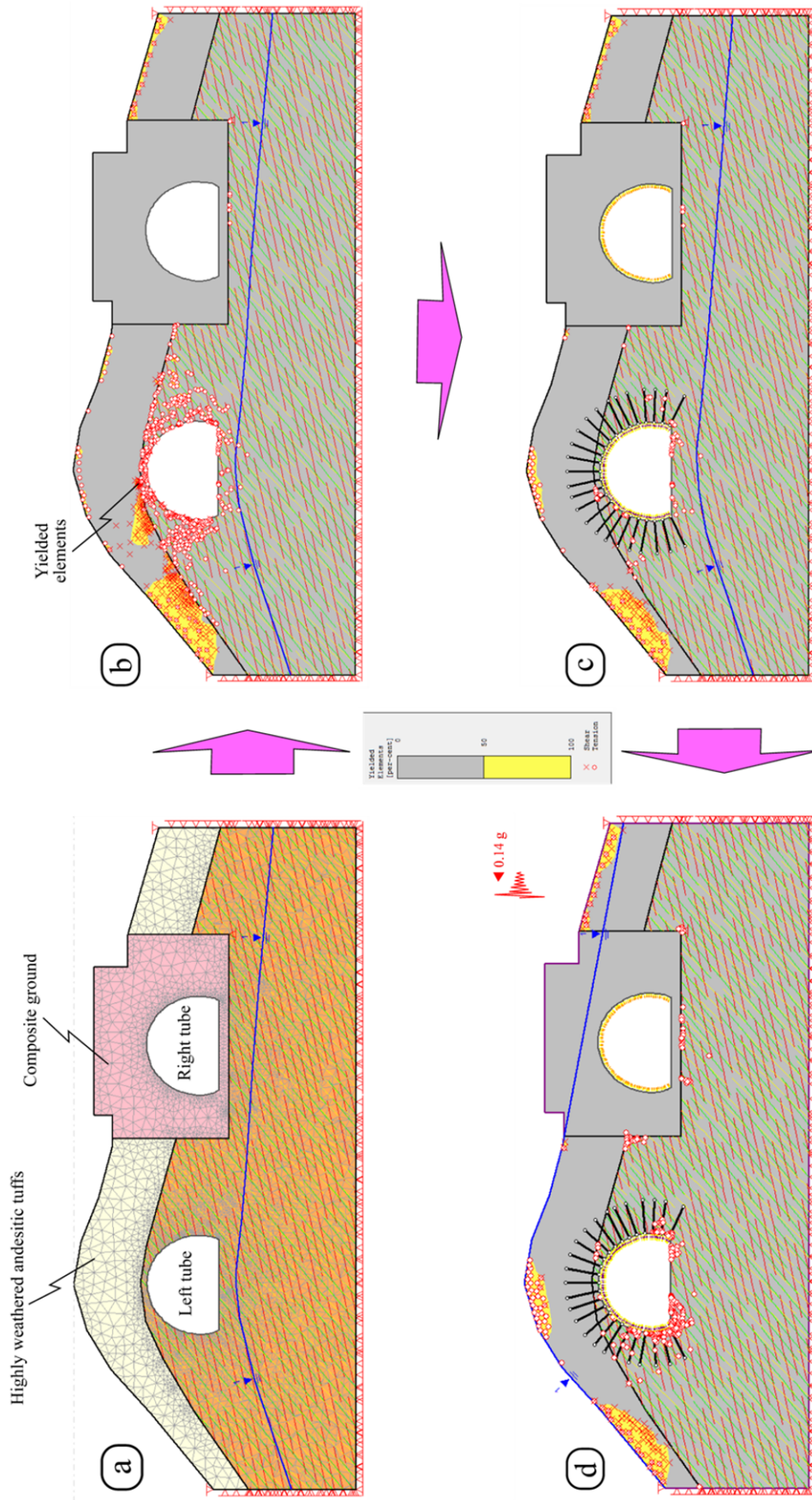


**Figure 10** Numerical analyses showing the plastic zones and yielded elements developed along the X-X' section for the unsupported and supported cases.

**Table 9** Stresses, displacements and maximum thickness of the plastic zones for the unsupported and supported cases along the X-X' section

		Unsupported case		Supported case (Static)		Supported case (Dynamic)	
		Left tube	Right tube	Left tube	Right tube	Left tube	Right tube
Roof	$\sigma_1$ (MPa)	1.75	0.25	0.45	0.25	0.40	0.24
	$\sigma_3$ (MPa)	0.02	0.02	0.09	0.09	0.10	0.06
Floor	$\sigma_1$ (MPa)	0.25	0.25	0.25	0.25	0.08	0.24
	$\sigma_3$ (MPa)	0.02	0.02	0.00	0.00	0.02	0.02
Left wall	$\sigma_1$ (MPa)	1.00	0.50	0.45	0.25	0.24	0.32
	$\sigma_3$ (MPa)	0.01	0.02	0.04	0.04	0.02	0.06
Right wall	$\sigma_1$ (MPa)	2.00	0.50	0.45	0.25	0.48	0.40
	$\sigma_3$ (MPa)	0.02	0.02	0.14	0.09	0.10	0.06
	$T_{pl}$ (m)	11.69	0.00	0.00	0.00	1.94	0.00
	$U_t$ (m)	0.0521		0.0439		0.0411	
$\sigma_1$ : Maximum principle stress (MPa)				$U_t$ : Maximum total displacement (m)			
$\sigma_3$ : Minimum principle stress (MPa)				$T_{pl}$ : Maximum thickness of plastic zone (m)			

(2) The findings obtained from FEM-SSR analyses showed that the main triggering factors of the failure are insufficient initial support design and weathering of lithology. Thus, the rock filling retaining wall improved with jet grout columns and reinforced slope benching are recommended as remedial measures to prevent the failure. After installing the support elements, the SRF value increased from 0.83 to 2.80.

### Acknowledgements

Authors would like to express their sincerest gratitude to the editor and reviewers. Thanks are due to the Academic Writing and Translation Office of Recep Tayyip Erdogan University for improving the language of the manuscript. The

(3) Finite element method (FEM) was undertaken to check the validity of the empirical preliminary tunnel support requirements obtained by the Q system. According to results acquired from the numerical analyses, it was found that the empirical support design is enough to reduce the maximum thickness of the plastic zones occurred in the roof and walls of the left tube.

author gratefully acknowledges Geological Engineer Aytuna SAYIN from the Turkish General Directorate of Highways for the office work associated with this study.

### References

Abramson LW, Lee TS, Sharma S, Boyce GM (2001) Slope stability and stabilization methods, 2nd edn. Wiley, New York. p 736.

Ahmadi M, Eslami M (2011) A New Approach to plane failure of rock slope stability based on water flow velocity in discontinuities for the Latian dam reservoir landslide. *Journal of Mountain Science* 8(2): 124-130. DOI: [10.1007/s11629-011-2088-5](https://doi.org/10.1007/s11629-011-2088-5)

Akgun A (2011) Assessment of possible damaged areas due to landslide-induced waves at a constructed reservoir using empirical approaches: Kurtun (North Turkey) dam reservoir area. *Natural Hazards and Earth System Sciences* 11(5): 1341-1350. DOI: [10.5194/nhess-11-1341-2011](https://doi.org/10.5194/nhess-11-1341-2011)

Akgun A, Bulut F (2007) GIS-based landslide susceptibility for Arsin-Yomra (Trabzon, North Turkey) region. *Environmental Geology* 51: 1377-1387. DOI: [10.1007/s00254-006-0435-6](https://doi.org/10.1007/s00254-006-0435-6)

Alemdag S, Akgun A, Kaya A, Gokceoglu C (2014) A large and rapid planar failure: causes, mechanism and consequences (Mordut, Gumushane, Turkey). *Arabian Journal of Geosciences* 7: 1205-1221. DOI: [10.1007/s12517-012-0821-1](https://doi.org/10.1007/s12517-012-0821-1)

Alemdag S, Kaya A, Karadag M, et al. (2015) Utilization of the limit equilibrium and finite element methods for the stability analysis of the slope debris: an example of the Kalebasi district (NE Turkey). *Journal of African Earth Sciences* 106: 134-146. DOI: [10.1016/j.jafrearsci.2015.03.010](https://doi.org/10.1016/j.jafrearsci.2015.03.010)

ASTM (2000) Standard Test Methods for Prebored Pressuremeter Testing in Soils (Withdrawn 2016). ASTM D4719-07, West Conshohocken, PA.

ASTM (2009) Standard test methods for laboratory determination of density (unit weight) of soil specimens. ASTM D7263-09, West Conshohocken, PA.

ASTM (2011) Standard practice for classification of soils for engineering purposes (Unified Soil Classification System). ASTM D2487-11, West Conshohocken, PA.

- Barton N (2002) Some new Q-value correlations to assist in site characterization and tunnel design. *International Journal of Rock Mechanics and Mining Sciences* 39(1): 185-216. DOI: [10.1016/S1365-1609\(02\)00011-4](https://doi.org/10.1016/S1365-1609(02)00011-4)
- Barton NR (1972) A model study of rock-joint deformation. *International Journal of Rock Mechanics and Mining Sciences* 9: 579-602.
- Barton NR, Bandis SC (1990) Review of predictive capabilities of JRC-JCS model in engineering practice. In: *Proceedings of the International Symposium on Rock Joints*, Loen. pp 603-610.
- Barton NR, Lien R, Lunde J (1974) Engineering classification of rock masses for the design of tunnel support. *Rock Mechanics* 4: 189-239.
- Beer G (1985) An isoparametric joint/interface element for finite element analysis. *International Journal for Numerical Methods in Engineering* 21(4): 585-600. DOI: [10.1002/nme.1620210402](https://doi.org/10.1002/nme.1620210402)
- Bieniawski ZT (1989) *Engineering Rock Mass Classifications*. Wiley, New York. p 251.
- Bishop AW (1955) The use of the slip circle in the stability analysis of slopes. *Geotechnique* 5: 7-17.
- Bishop AW, Morgenstern N (1960) Stability coefficients for earth slopes. *Geotechnique* 10(4): 129-150.
- Borja-Baeza RC, Esteban-Chávez O, Marcos-López J, et al. (2006) Slope instability on pyroclastic deposits: landslide distribution and risk mapping in Zacapoaxtla, Sierra Norte De Puebla, Mexico. *Journal of Mountain Science* 3(1): 1-19. DOI: [10.1007/s11629-006-0001-4](https://doi.org/10.1007/s11629-006-0001-4)
- Bowles JE (1988) *Foundation analysis and design*. McGraw-Hill Book Company, New York.
- Brill GT, Burke GK, Ringen AR (2003) A ten year perspective of jetgrouting: advancements in applications and technology. *Proceedings of the 3rd International Conference – Grouting and Ground Treatment*, New Orleans 1(120): 218-235.
- Bulut F, Boynukahn S, Tarhan F, Ataoglu E (2000) Reliability of landslide isopleth maps. *Bulletin of Engineering Geology and the Environment* 58: 95-98. DOI: [10.1007/s100640050002](https://doi.org/10.1007/s100640050002)
- Cai M, Kaiser PK, Tasaka Y, Minami M (2007) Determination of residual strength parameters of jointed rock masses using the GSI system. *International Journal of Rock Mechanics and Mining Sciences* 4(2): 247-265. DOI: [10.1016/j.ijrmms.2006.07.005](https://doi.org/10.1016/j.ijrmms.2006.07.005)
- Capkinoglu S (1981) *Geology of the district between Borcka and Cavuslu (Hopa)*. MSc. Thesis, Karadeniz Technical University.
- Deere DU (1964) Technical description of rock cores for engineering purposed. *Rock Mechanics and Rock Engineering* 1: 17-22.
- Del Gaudio V, Trizzino R, Calcagnile G, et al (2000) Landsliding in seismic areas: the case of the Acquara-Vadoncello landslide (southern Italy). *Bulletin of Engineering Geology and the Environment* 59: 23-37. DOI: [10.1007/s100640000054](https://doi.org/10.1007/s100640000054)
- Du GL, Zhang YS, Iqbal J, et al. (2017) Landslide susceptibility mapping using an integrated model of information value method and logistic regression in the Bailongjiang watershed, Gansu Province, China. *Journal of Mountain Science* 14(2):249-268. DOI: [10.1007/s11629-016-4126-9](https://doi.org/10.1007/s11629-016-4126-9)
- Fahimifar A, Abdolmaleki A, Soltani P (2013) Stabilization of rock slopes using geogrid boxes. *Arabian Journal of Geoscience* 7(2): 609-621. DOI: [10.1007/s12517-012-0755-7](https://doi.org/10.1007/s12517-012-0755-7)
- Fell R, Walker BF, Finlay PJ (1996) Estimating the probability of landsliding. *Proceedings 7th Australian New Zealand Conference on Geomechanics*, Adelaide, Institution of Engineers Australia, Canberra. pp 304-311.
- Fellenius W (1936) Calculation of the stability of earth dams. *Proc.Transactions of the 2nd Congress on Large Dams*, International Commission on Large Dams of the World Power Conference 4: 445-462.
- Gardner JS, Sazuk E (2004) Systems for hazards identification in high mountain areas: An example from the Kullu District, western Himalaya. *Journal of Mountain Science* 1(2): 115-127. DOI: [10.1007/BF02919334](https://doi.org/10.1007/BF02919334)
- Genç S (1993) Structural and geomorphological aspects of the Catak landslide, NE Turkey. *Quarterly Journal of Engineering Geology and Hydrogeology* 26(2): 99-108. DOI: [10.1144/GSL.Q.JEG.1993.026.02.02](https://doi.org/10.1144/GSL.Q.JEG.1993.026.02.02)
- Ghaboussi J, Wilson EL, Isenberg J (1973) Finite element for rock joints and interfaces. *Journal of the Soil Mechanics and Foundations Division, ASCE* 99(M10): 833-848.
- Goodman RE, Taylor RL, Brekke TL (1968) A model for the mechanics of jointed rock. *Journal of the Soil Mechanics and Foundations Division, ASCE* 637-659.
- Griffiths DV, Lane PA (1999) Slope stability analysis by finite elements. *Geotechnique* 49(3): 387-403. DOI: [10.1680/geot.1999.49.3.387](https://doi.org/10.1680/geot.1999.49.3.387)
- Guatteri G, Kauschinger JL, Doria AC, Perry EB (1988) Advances in the construction and design of jetgrouting methods in South America. *Proceedings of the International Conference on Case Histories in Geotechnical Engineering* 5(32): 1037-1046.
- Guven IH (1993) 1/25000 Scale geology map of eastern Pontides. *Mineral Research and Exploration Institute of Turkey (MTA) Publication*.
- Guzzetti F, Carrara A, Cardinali M, Reichenbach P (1999) Landslide hazard evaluation: a review of current techniques and their application in a multi-scale study, Central Italy. *Geomorphology* 31: 181-216. DOI: [10.1016/S0169-555X\(99\)00078-1](https://doi.org/10.1016/S0169-555X(99)00078-1)
- Hammah RE, Yacoub TE, Corkum B, Curran JH (2008) The practical modelling of discontinuous rock masses with finite element analysis. In *Proceedings of the 42nd US Rock Mechanics Symposium and 2nd US Canada Rock Mechanics Symposium*, San Francisco.
- Hammah RE, Yacoub TE, Curran JH (2006) Investigating the performance of the shear strength reduction (SSR) method on the analysis of reinforced slopes. In: *Proceedings of the 59th Canadian Geotechnical Conference*, Vancouver.
- Hart RD, Detournay C, Cundall PA (2008) Continuum and distinct element modeling in geo-engineering. In: Cundall PA (ed) *Proceedings First FLAC/DEM Symposium*, Minneapolis. p 698.
- Hoek E, Carranza-Torres C, Corkum B (2002) Hoek-Brown failure criterion-2002 edition. *Proceedings of NARMS-TAC2002, Mining Innovation and Technology*, Toronto, Canada. pp 267-273.
- Hoek E, Carter TG, Diederichs MS (2013) Quantification of the Geological Strength Index chart. *47th US Rock Mechanics and Geomechanics Symposium*, San Francisco, USA.
- ISRM (2007) The complete ISRM suggested methods for rock characterization, testing and monitoring: 1974–2006. *International Society of Rock Mechanics Turkish National Group*, Ankara, Turkey. p 628.
- Janbu N (1954) Stability analysis of slopes with dimensionless parameters. *Soil Mechanics Series No. 46*, Harvard University. p 81.
- Ju NP, Huang J, Huang RQ, et al. (2015) A real-time monitoring and early warning system for landslide in southwest China. *Journal of Mountain Science* 12(5): 1219–1228. DOI: [10.1007/s11629-014-3307-7](https://doi.org/10.1007/s11629-014-3307-7)
- Karaman K (2013) Evaluation of rock slope stability by different methods (Unye, Ordu). *Journal of Geological Engineering* 37: 27-47.
- Karaman K, Ercikdi B, Kesimal A (2013) Assessment of slope stability and excavatability of rocks in a limestone quarry. *Earth Sciences Research Journal* 17: 169-181.
- Kaya A (2012) The geotechnical investigation of the Cankurtaran (Hopa-Artvin) tunnel alignment and surrounding area. Ph.D. Thesis, Karadeniz Technical University.
- Kaya A (2016) Geotechnical assessment of a slope stability problem in the Citlakale residential area (Giresun, NE Turkey), *Bulletin of Engineering Geology and the Environment*. DOI: [10.1007/s10064-016-0896-0](https://doi.org/10.1007/s10064-016-0896-0)
- Kaya A, Akgün A, Karaman K, Bulut F (2015) Understanding the mechanism of a slope failure on a nearby highway tunnel route

- by different slope stability analysis methods: a case from NE Turkey. *Bulletin of Engineering Geology and the Environment* 75(3): 945-958. DOI: [10.1007/s10064-015-0770-5](https://doi.org/10.1007/s10064-015-0770-5)
- Kaya A, Alemdağ S, Dağ S, Gürocak Z (2016) Stability assessment of high-steep cut slope debris on a landslide (Gumushane, NE Turkey). *Bulletin of Engineering Geology and the Environment* 1(75): 89-99. DOI: [10.1007/s10064-015-0753-6](https://doi.org/10.1007/s10064-015-0753-6)
- Kaya A, Bulut F (2013) Stability analyses of tunnels excavated in weak rock masses using empirical and numerical methods. *Journal of Geological Engineering* 37(2): 103-116.
- Ketin I (1966) Tectonic units of Anatolia. *Journal of General Directorate of Mineral Research and Exploration (MTA)* 66: 23-34.
- KGM (2013) Specification for highway works (In Turkish). Turkish General Directorate of Highways, Ankara.
- Li AJ, Merifield RS, Lyamin AV (2011) Effect of rock mass disturbance on the stability of rock slopes using the Hoek-Brown failure criterion. *Computers and Geotechnics* 38(2011): 546-558. DOI: [10.1016/j.compgeo.2011.03.003](https://doi.org/10.1016/j.compgeo.2011.03.003)
- Li X (2007) Finite element analysis of slope stability using a nonlinear failure criterion. *Computers and Geotechnics* 34: 127-136. DOI: [10.1016/j.compgeo.2006.11.005](https://doi.org/10.1016/j.compgeo.2006.11.005)
- Lowe J, Karafiath L (1959) Stability of earth dams upon drawdown. *Proc. 1st PanAmerican Conference on Soil Mechanics and Foundation Engineering* 2: 537-552.
- Lugeon M (1933) Dams and geological field investigation methods and permeabilization. *Literature of Paris University, Paris. (Barrages et geologic methods de recherche' terrasement et un permeabilisation. Litrairedes Universite, Paris.)*
- Manouchehrian A, Gholamnejad J, Sharifzadeh M (2014) Development of a model for analysis of slope stability for circular mode failure using genetic algorithm. *Environmental Earth Sciences* 71(3): 1267-1277. DOI: [10.1007/s12665-013-2531-8](https://doi.org/10.1007/s12665-013-2531-8)
- Matsui T, Sam KC (1992) Finite element slope stability analysis by shear strength reduction technique. *Soils and Foundations* 32(1): 59-70.
- Menard L (1956) An apparatus for measuring the strength of soils in place. *Master of Science Thesis, University of Illinois*
- Menard L (1975) Interpretation and application of pressuremeter test results to foundation design. *Sols-Soils No: 26*
- MGM (2016) Turkish State Meteorological Servive. <http://www.mgm.gov.tr/iklim/iklim-siniflandirmalari.aspx>. Accessed 23 September 2016
- Mining Research Laboratories (Canada) (1977) Pit Slope Manual: Supplement 5-1, Plane Shear Analysis. Ottawa: Canada Centre for Mineral and Energy Technology, pp 16-77.
- Mohr O (1900) Which conditions determine the elasticity limit and failure of a material? *Journal of the Association of German Engineers (Welche umstande bedingen die elastizitatsgrenze und den bruch eines materials? Zeit des Ver Deut Ing)* 44: 1524-1530.
- Morgenstern NR, Price VE (1967) A numerical method for solving the equations of stability of general slip surfaces. *Computer Journal* 9(4): 388-393.
- Ö-NORM B2203 (1994) Underground construction work contract standard, Austrian standards, Austria. (Untertagebauarbeiten werkvertragsnorm, Österreichischer Normen, Österreich).
- Pelizza S, Peila D (1993) Soil and rock reinforcements in tunnelling. *Tunnelling and Underground Space Technology* 8(3):357-372. DOI: [10.1016/0886-7798\(93\)90020-V](https://doi.org/10.1016/0886-7798(93)90020-V)
- Rocscience Inc. (2002) RocLab version 1.0 - rock mass strength analysis using the generalized Hoek-Brown failure criterion. Toronto, ON. <http://www.rocsience.com>
- Rocscience Inc. (2004) Dips Version 5.0 - graphical and statistical analysis of orientation data. Toronto, ON. <http://www.rocsience.com>
- Rocscience Inc. (2010) Slide version 6.0 - 2D limit equilibrium slope stability analysis, Toronto, ON. <http://www.rocsience.com>
- Rocscience Inc. (2011) Phase<sup>2</sup> version 8.0 - finite element analysis for excavations and slopes, Toronto, ON. <http://www.rocsience.com>
- Sancio RT (1981) The use of back-calculations to obtain shear and tensile strength of weathered rocks. *Proceedings of the International Symposium on Weak Rock, Tokyo*, pp 647-652.
- Sarkar S, Anbalagan R (2008) Landslide hazard zonation mapping and comparative analysis of hazard zonation maps. *Journal of Mountain Science* 5: 232-240. DOI: [10.1007/s11629-008-0172-2](https://doi.org/10.1007/s11629-008-0172-2)
- Sarma SK (1973) Stability analysis of embankments and slopes. *Geotechnique* 23(3): 423-433.
- Shukra R, Baker R (2003) Mesh geometry effects on slope stability calculation by FLAC strength reduction method-linear and non-linear failure criteria. In (Brummer R, et al, eds.) *proceedings of the 3rd International FLAC Symposium, Sudbury, Ontario, Canada*. pp 109-116.
- Spencer E (1967) A method of analysis of the stability of embankments assuming parallel inter-slice forces. *Geotechnique* 17(1): 11-267.
- Turner KA, Schuster RL (1996) *Landslides: investigation and mitigation*. National Academy Press, Washington DC. p 672.
- Ulusay R, Tuncay E, Sonmez H, Gokceoglu C (2004) An attenuation relationship based on Turkish strong motion data and iso-acceleration map of Turkey. *Engineering Geology* 74 (3-4): 265-291. DOI: [10.1016/j.enggeo.2004.04.002](https://doi.org/10.1016/j.enggeo.2004.04.002)
- USCE (1970) *Engineering and design: stability of earth and rock-fill dams*. Engineer Manual EM 1110-2-1902, Department of the Army, Corps of Engineers, Office of the Chief of Engineers, Washington DC.
- Wang XF, Zhang DS, Zhang CG, et al. (2013) Mechanism of mining-induced slope movement for gullies overlaying shallow coal seams. *Journal of Mountain Science* 10(3): 388-397. DOI: [10.1007/s11629-013-2455-5](https://doi.org/10.1007/s11629-013-2455-5)
- Wang XG, Wang JD, Gu TF, et al. (2017) A modified Hoek-Brown strength criterion considering the damage to reservoir bank slope rocks under water saturation-dehydration circulation. *Journal of Mountain Science* 14(4): 771-781. DOI: [10.1007/s11629-016-4206-x](https://doi.org/10.1007/s11629-016-4206-x)
- Wyllie DC, Mah CW (2004) *Rock slope engineering*. Spon Press, New York.
- Yang T, Yeung MC, Yang B, et al. (2016) Three-dimensional stability of landslides based on local safety factor. *Journal of Mountain Science* 13(9): 1515-1526. DOI: [10.1007/s11629-016-3918-2](https://doi.org/10.1007/s11629-016-3918-2)